Supporting Information

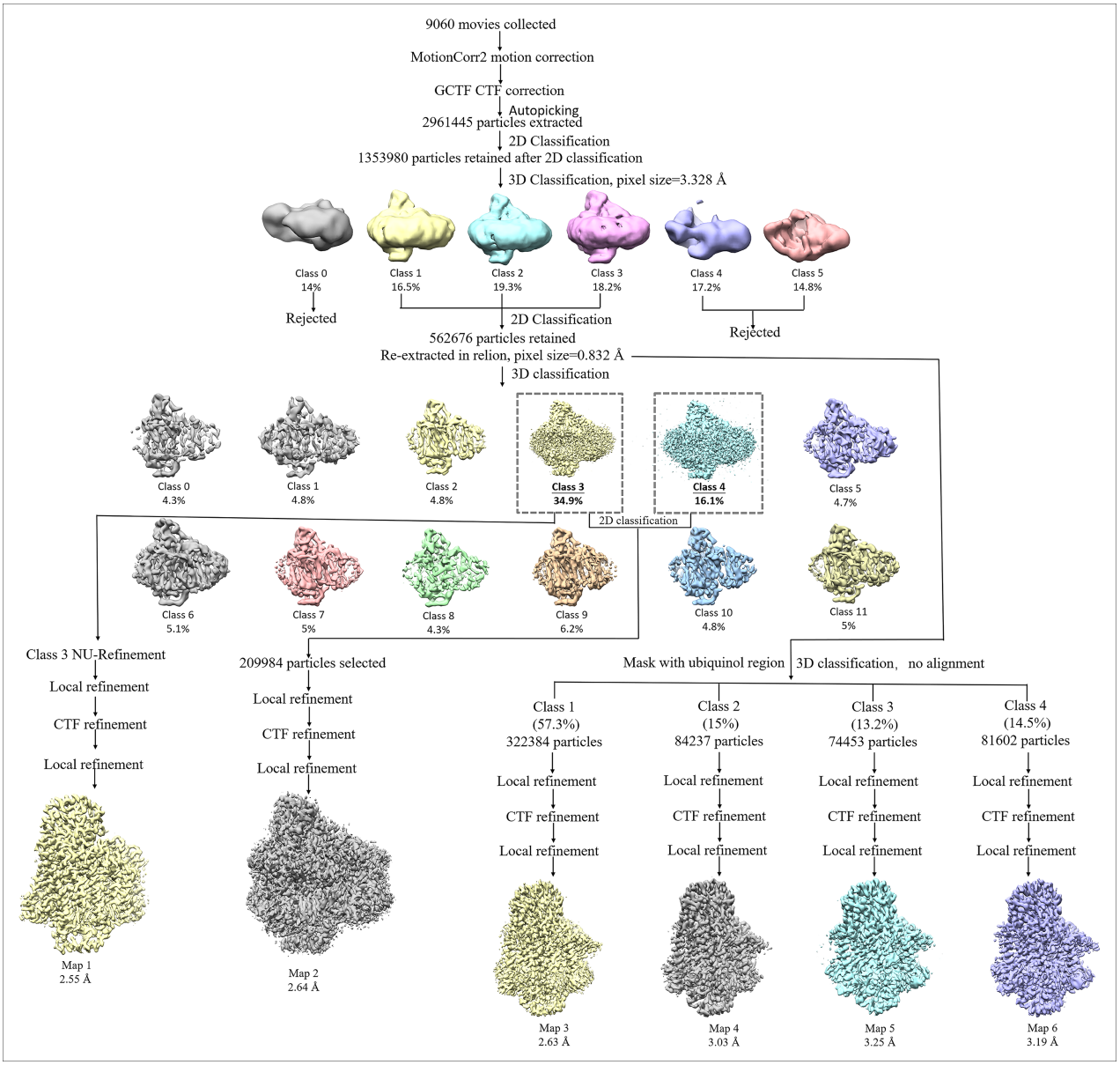

Figure S1. Classification and refinement of the cryo-EM maps for *E. Coli* cyt bo_3 purified in SMA. The workflow, implemented in Relion 3.0.7 and cryoSPARC v2.15.0, was used to obtain the Map 1 of the whole complex at 2.55 Å resolution. The Map 2 of the whole complex, with the phospholipids, was obtained at 2.64 Å resolution; the Maps 3 to 6 showing a dynamic UQ8 binding site, were rebuilt at 2.63 Å, 3.03 Å, 3.25 Å, and 3.19 Å resolution，respectively.

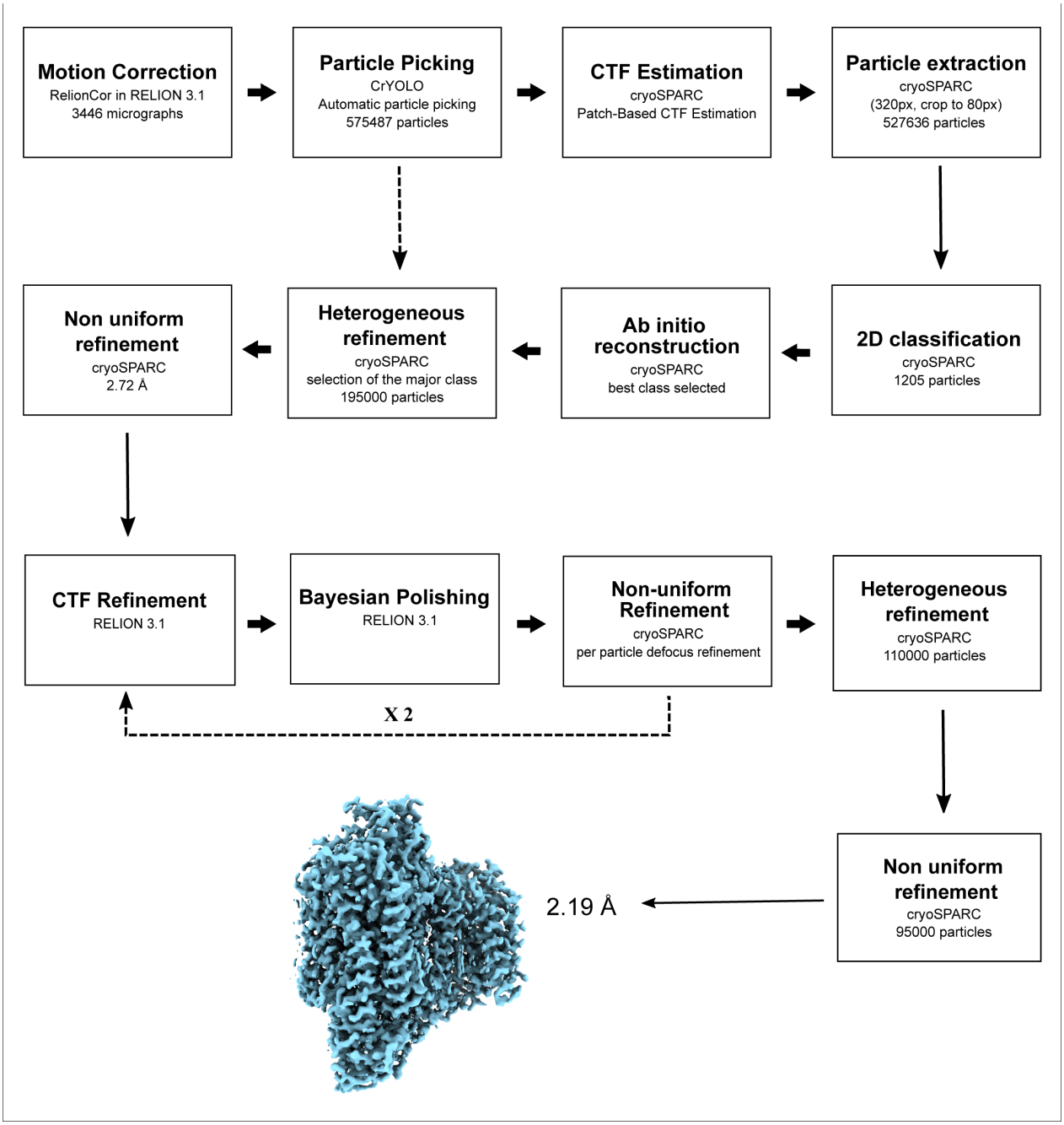

Figure S2. Classification and refinement of the cryo-EM maps for *E. Coli* cyt *bo*$_3$ purified in MSP nanodiscs. The workflow, implemented in CrYOLO, Relion 3.1 and cryoSPARC v3.2.0, was used to obtain the map of the complex at 2.19 Å resolution.

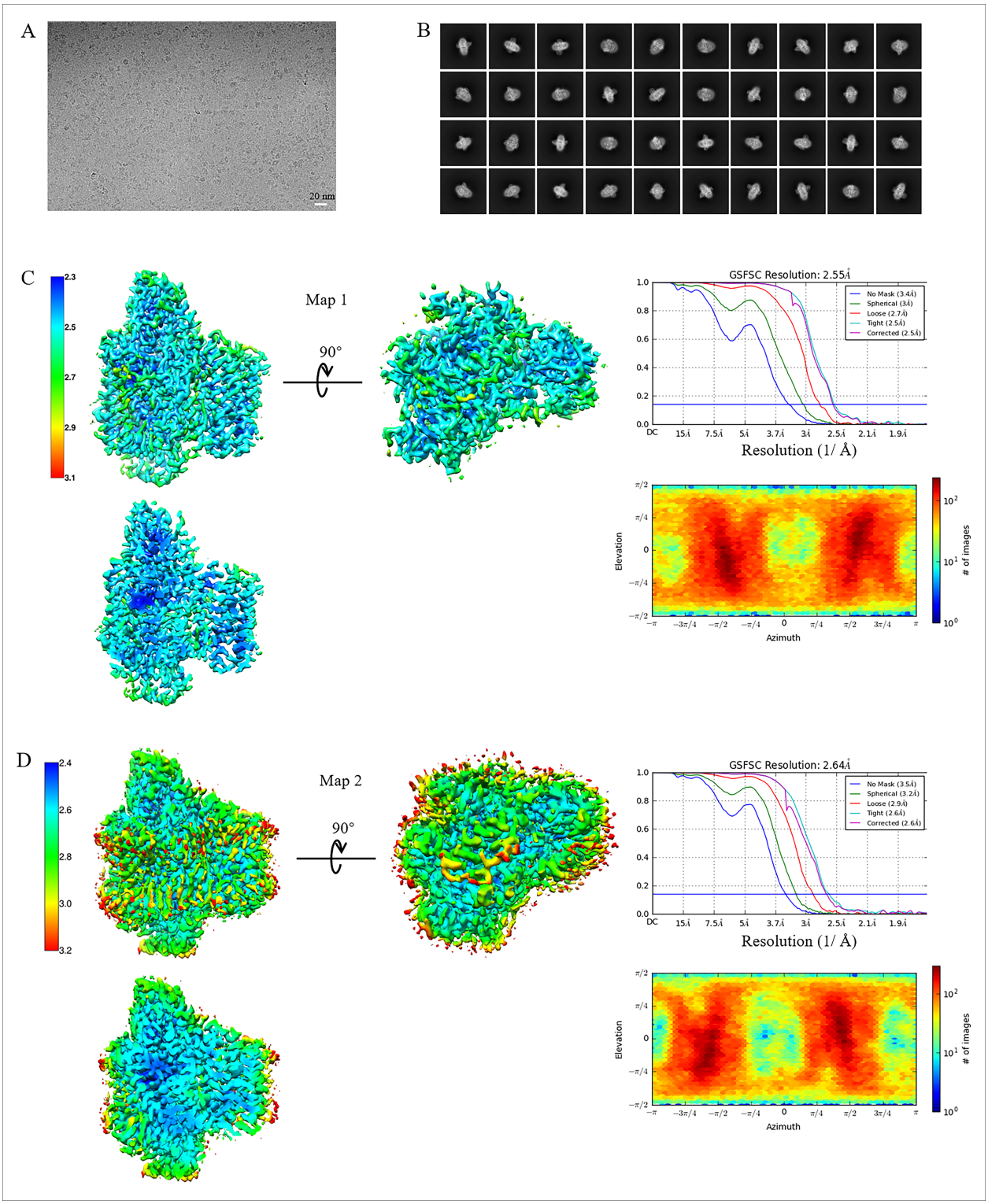

Figure S3. Single-particle cryo-EM of *E. coli* cyt *bo₃* purified in SMA. (A) Summary of an aligned movie of *E. coli* cyt *bo₃* in SMA. The scale bar is 20 nm. (B) Class averages after final

round of two-dimensional classification, sorted in descending order by the number of particles in each class. (C) Overview of the final cryoSPARC B-factor-sharpened map of *E. coli* cyt bo_3. Map 1, colored by local resolution in Å, as calculated by ResMap with full views (upper lane) from different orientations and sliced view (lower lane). (Top Right) Gold standard FSC curve from cryoSPARC. (Bottom Right) Euler angle orientation distribution of particles from cryoSPARC. (D) Local-resolution map, FSC curve and Euler angle orientation distribution for Map 2; both were calculated as represented in (C).

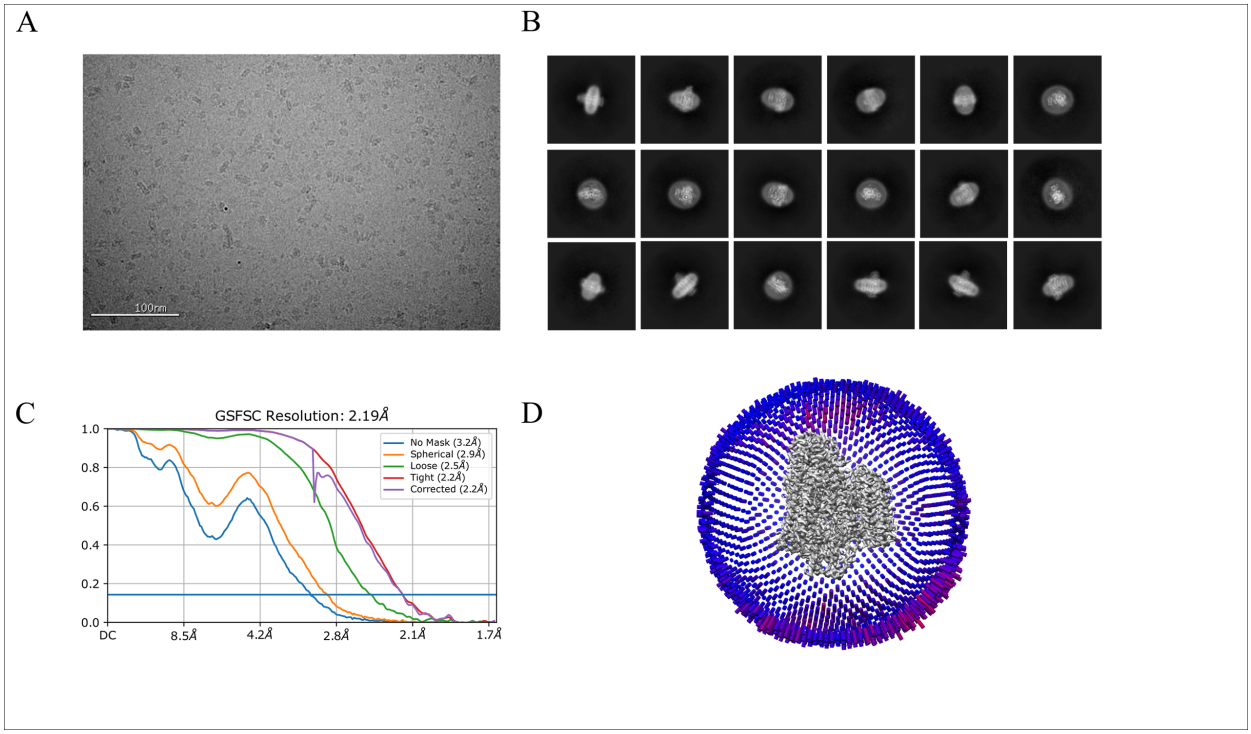

Figure S4. Single-particle cryo-EM of *E. Coli* cyt bo_3 in MSP nanodiscs. (A) Representative micrograph of *E. coli* cyt bo_3. The scale bar is 100 nm. (B) Class averages after final round of two-dimensional classification, sorted in descending order by number of particles in each class. (C) Gold standard FSC curve from cryoSPARC. (D) Orientation plot of particles included in the final 3D reconstruction.

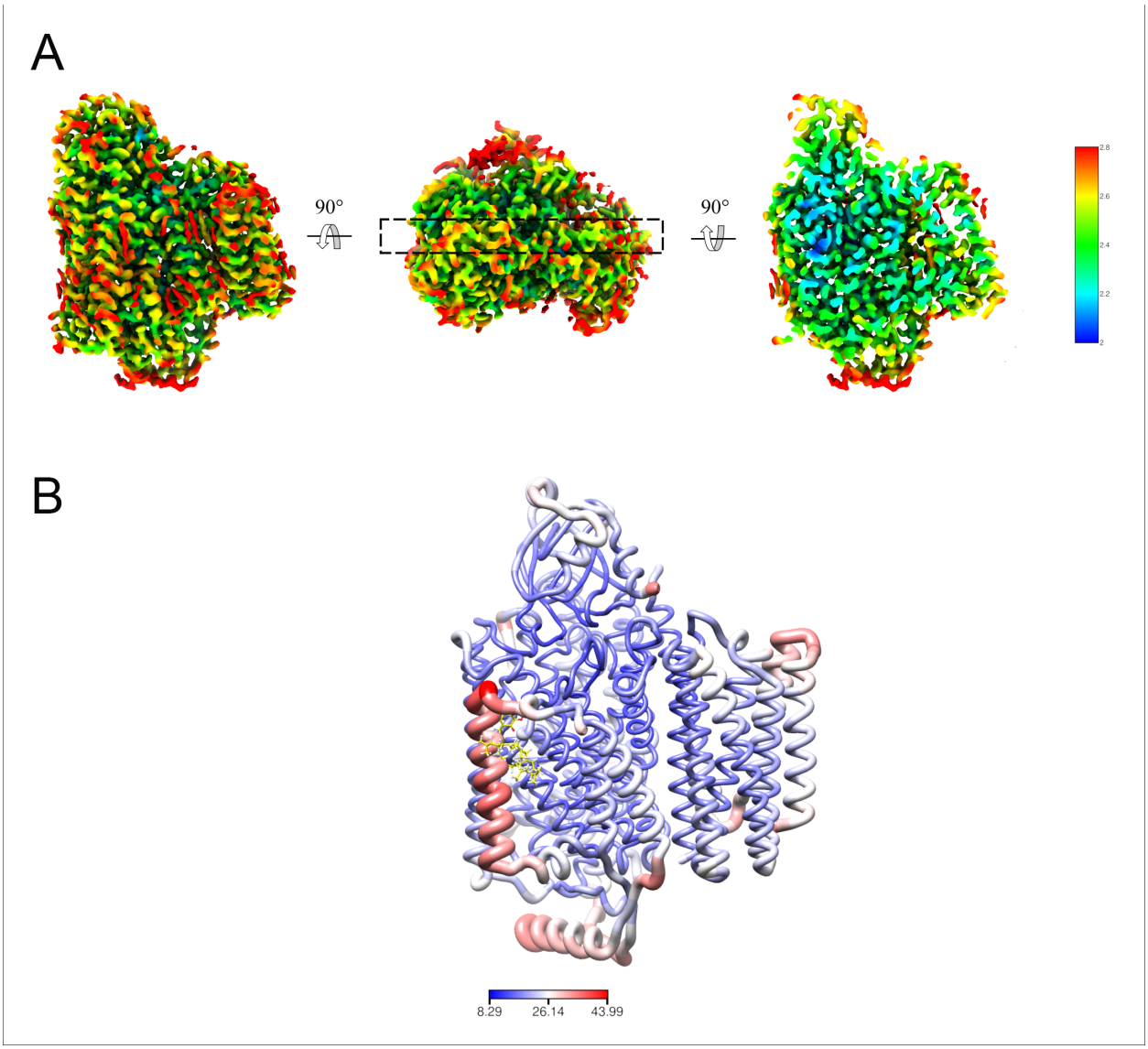

Figure S5. Local resolution and B-factor distributions. (A) Lateral, top, and plane view of cyt *bo*$_3$ EM structure in MSP. Local resolution distribution from 2 (blue) to 2.8 (red). (B) Worm-format representation of the B-factors for cyt *bo*$_3$ EM structure in MSP, B-factor distributions from 8.22 (blue) to 44 (red).

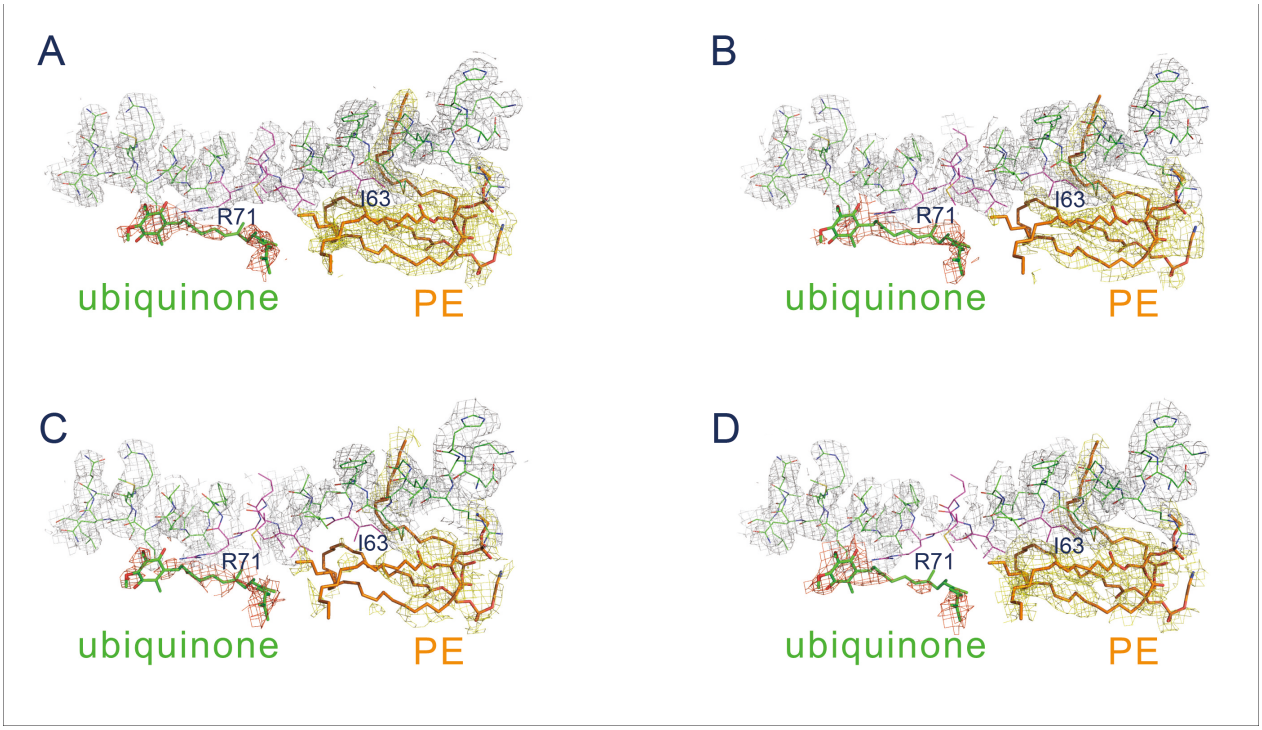

Figure S6. Conformational change of the bound ubiquinone, lipids and nearby residues in the SMA-purified protein. UQ8 is contoured at 5.5σ, PE at 5.0σ and amino acid residues at 6.5σ. (A) The map was rebuilt with 322384 particles with a resolution of 2.63 Å. The UQ8 has well defined head group density and good tail density. The nearby PEs and amino acid residues are well ordered. (B) The map was rebuilt with 84237 particles with a resolution 3.03 Å. The UQ8 has poor head group density, but well defined tail density. The nearby amino acid residues are well ordered, but the lipid tails have low density. (C) The map was rebuilt with 74453 particles with a resolution 3.25 Å. The UQ8, the lipid tails and residues I63, L67-R71 have low density. (D) The map was rebuilt with 81602 particles with a resolution 3.19 Å. The UQ8 and the residues L67-R71 have very low density, indicating high flexibility, but the density of lipid tails remain well defined.

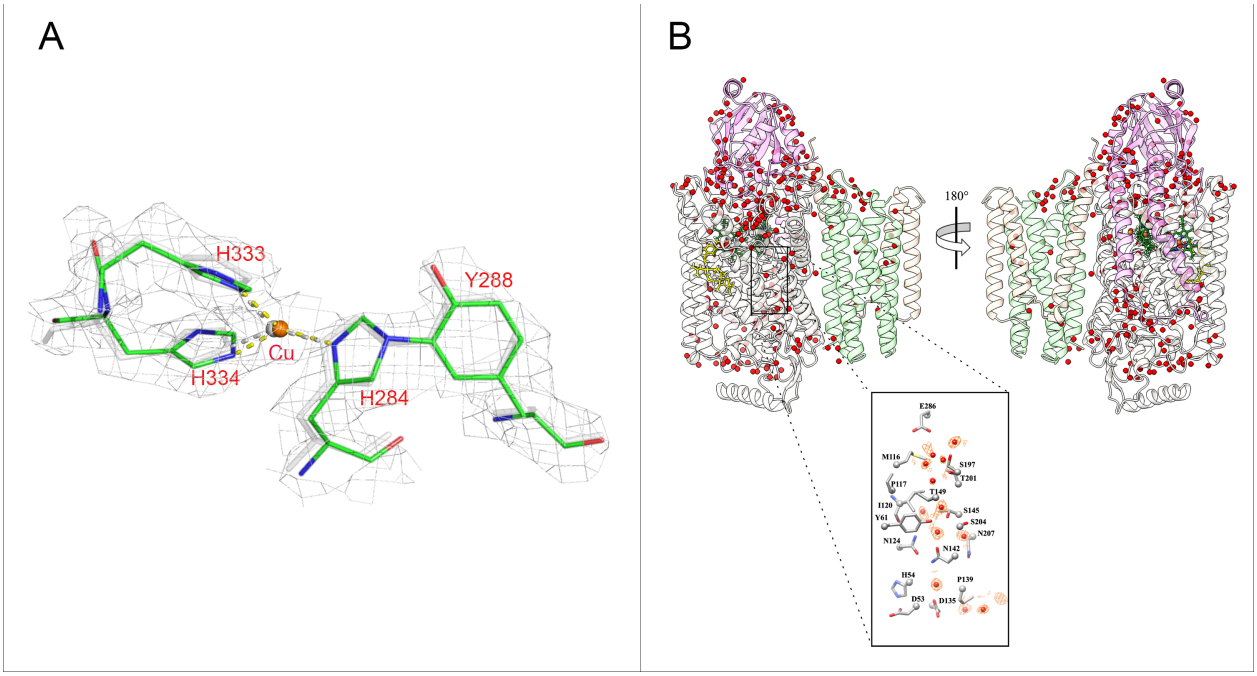

Figure S7. Crosslinked histidine-tyrosine and proton-conducting D-channel. (A) Superposition of the active sites for SMA purified cyt bo_3 model (green) and the *R. sphaeroides* cytochrome *c* oxidase model (white). The density suggests the histidine-tyrosine crosslink. (B) Water molecules. Structure of cyt bo_3 EM in MSP showing the ordered water molecules (red spheres, in yellow ubiquinone and in green the heme). A zoom of the amino acids that are part of the D-channel with the water molecules that occupy it.

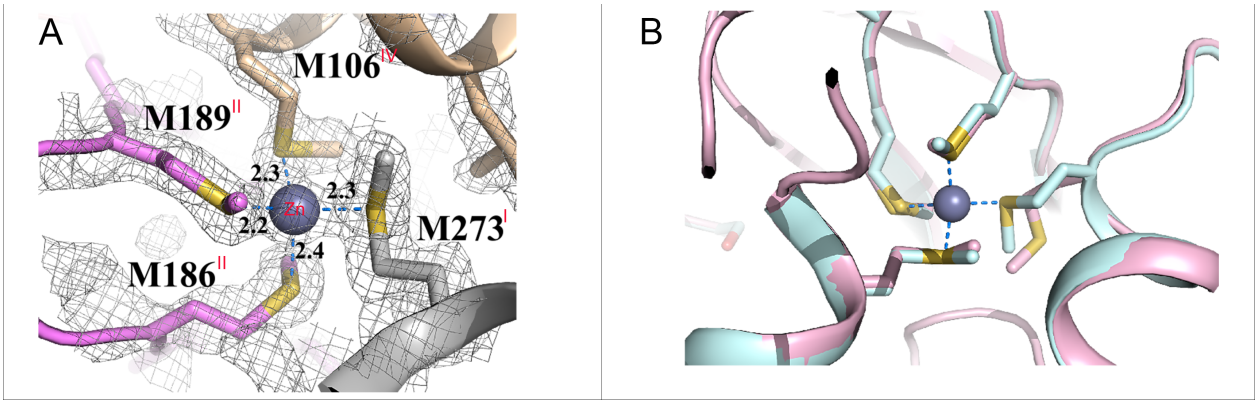

Figure S8. Zinc binding site. (A) Zinc binding site for cyt *bo*$_3$ model in MSP nanodiscs. Binding of Zn^{2+} is mediated by four methionines; M186 and M189 from subunit II, M106 from subunit IV, and M273 from subunit I. All the distances indicated in the figure are in Å. (B) Superposition of the zinc site for both cyt *bo*$_3$ model in MSP (light blue) and the cyt *bo*$_3$ model in SMA (pink).

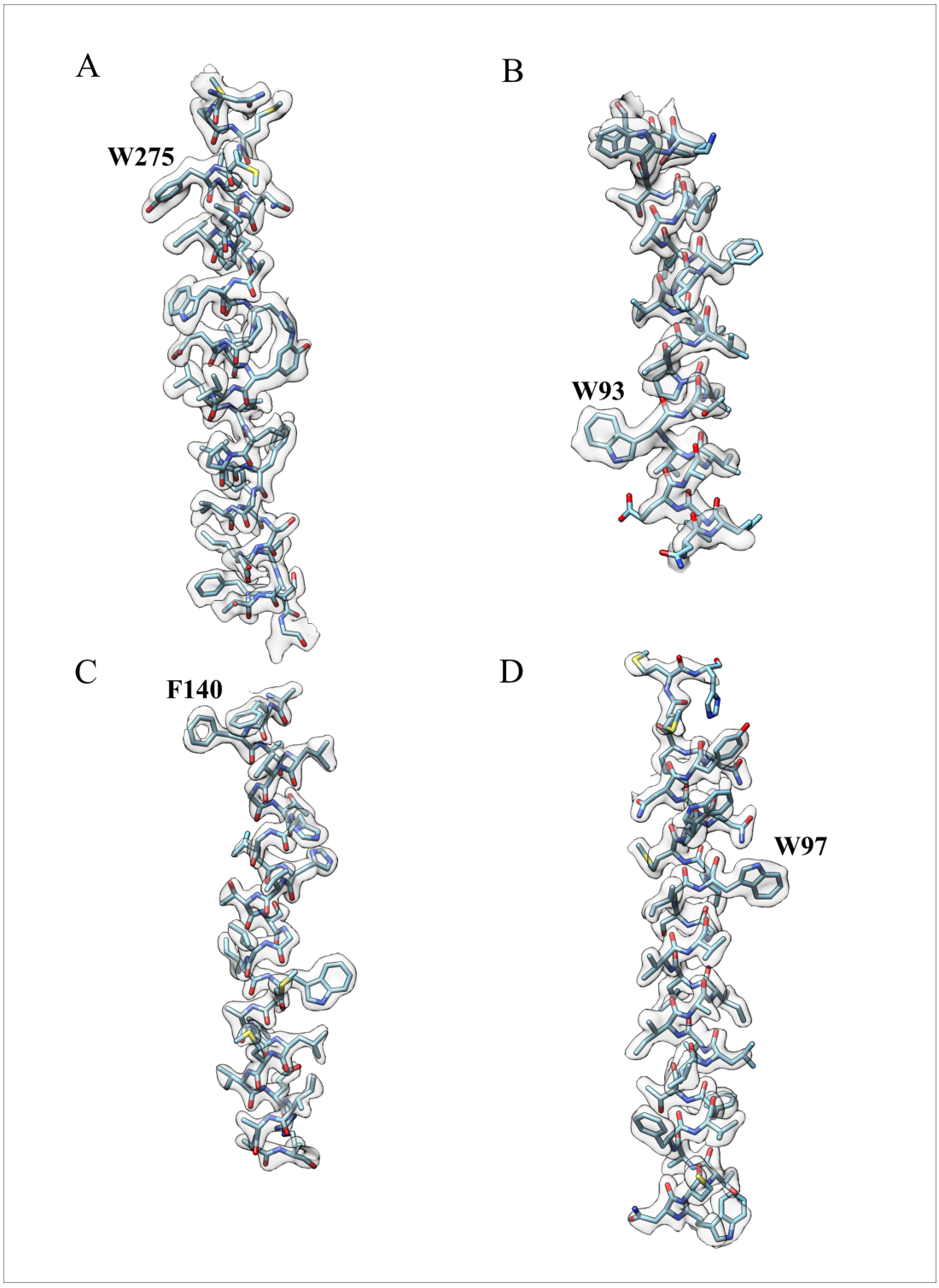

Figure S9. Representative densities of cyt *bo*$_3$ -selected regions. Panel A is from Subunit I; Panel B from Subunit II; Panel C from III and Panel D from Subunit IV.

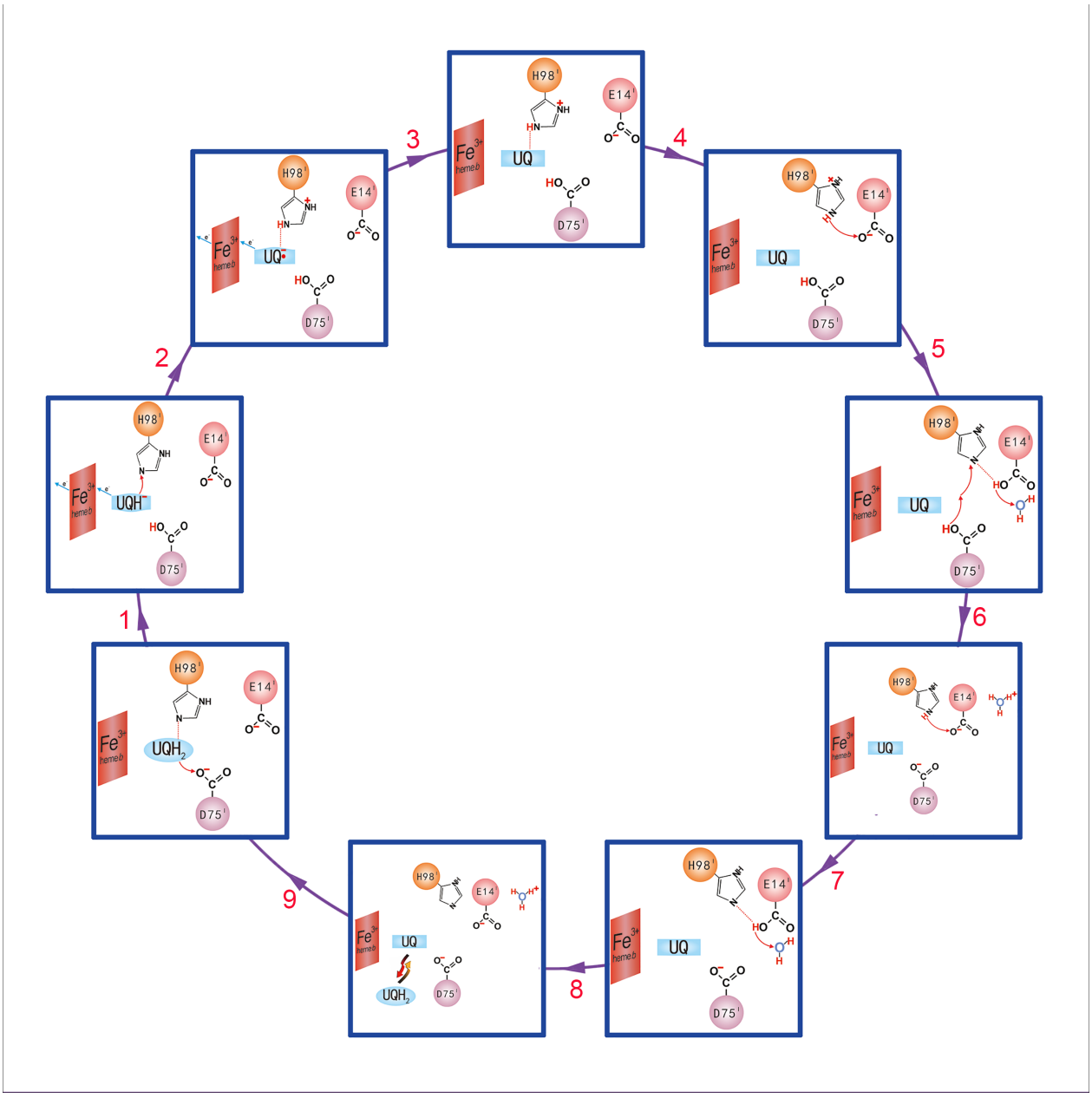

Figure S10. The sequence of electron and proton transfer.

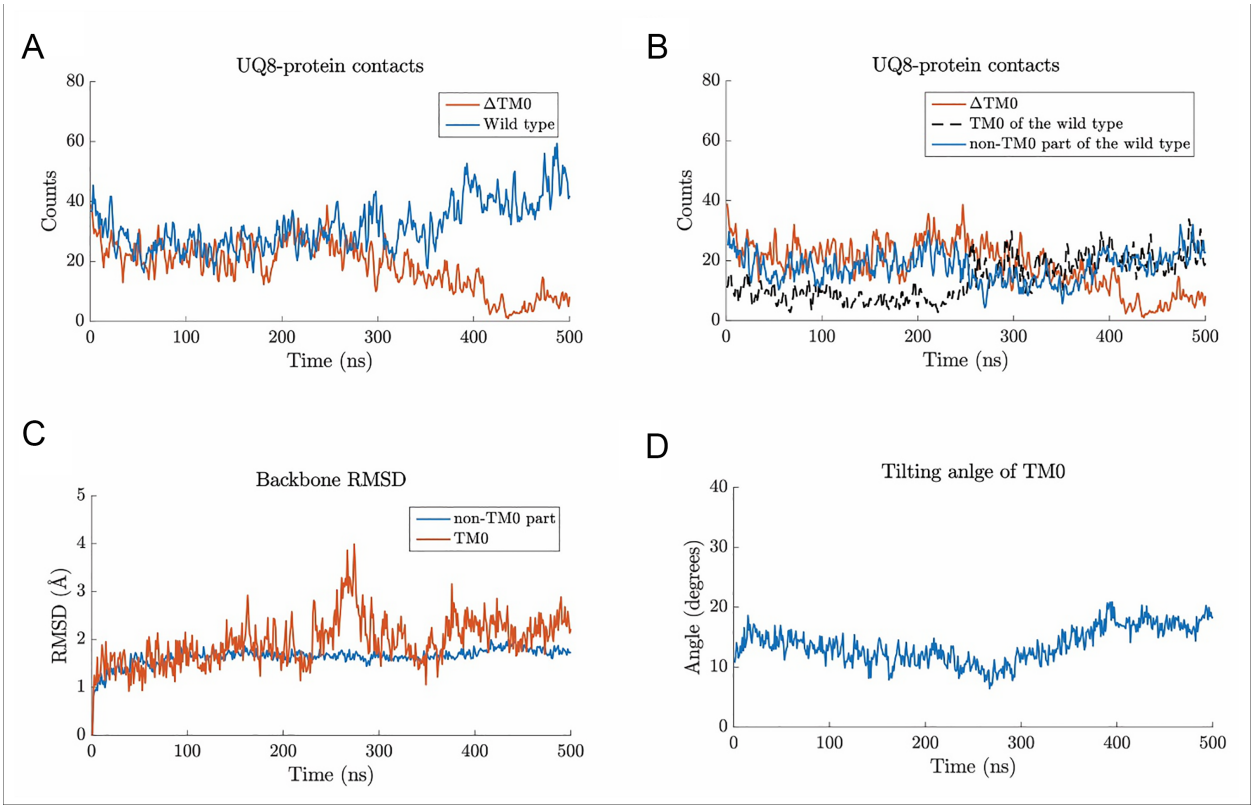

Figure S11. UQ8-cyt *bo*$_3$ contact analyses and flexibility of TM0. (A) The number of contacts made between the headgroup of UQ8 and cyt *bo*$_3$ along MD simulations. (B) A breakdown of the number of contacts shown in (A) into those made with TM0 and those made with the non-TM0 part of cyt *bo*$_3$. (C) RMSD for backbone atoms of the non-TM0 part of cyt *bo*$_3$ and that of TM0 for the wild type cyt *bo*$_3$. (D) Tilting angle of TM0 from the membrane normal for the wild type cyt *bo*$_3$. A tilting angle of 0 degree corresponds to having TM0 aligned parallel with the membrane normal, which is the *z* - axis during MD simulations.

Table S1. Cryo-EM data collection, refinement and validation statistics

	SMA-purified cyt *bo*$_3$ with best resolved ubiquinone (EMDB-30475) (PDB 7CUW)	SMA-purified cyt *bo*$_3$ with best resolved phospholipid molecules (EMDB-30474) (PDB 7CUQ)	SMA-purified cyt *bo*$_3$ with best resolved water molecules (EMDB-30471) (PDB 7CUB)	MSP nanodisc-reconstituted cyt *bo*$_3$ (EMDB-24265) (PDB 7N9Z)
Data collection and processing				
Magnification	105,000×	105,000×	105,000×	105,000x
Voltage (kV)	300	300	300	300
Electron exposure (e^-/Å2)	65	65	65	58
Defocus range (μm)	−1.2 to −2.0	−1.2 to −2.0	−1.2 to −2.0	−0.5 to −1.5
Pixel size (Å)	0.832	0.832	0.832	0.832
Symmetry imposed	C1	C1	C1	C1
Initial particle images (no.)	2961445	2961445	2961445	575487
Final particle images (no.)	322384	209984	193845	94681
Map resolution (Å)	2.63*	2.64*	2.55*	2.19*
FSC threshold	0.143	0.143	0.143	0.143
Refinement				
Initial model used	PDB 7CUB	PDB 7CUB	PDB 1FFT	PDB 1FFT
Model resolution (Å)	2.6	2.6	2.5	2.19
FSC threshold	0.143	0.143	0.143	0.143
Map sharpening B factor (Å^2)	-80.0	-96.4	-77.4	-65.5
Model composition				
Nonhydrogen atoms	9839	9834	9842	10473
Protein residues	1199	1199	1199	1202

Ligands	9	9	9	17
B factors (Å^2)				
Protein	43.24	111.51	31.51	19,36
Ligand	47.53	116.05	32.8	23,88
R.M.S. deviations				
Bond lengths (Å)	0.008	0.004	0.005	0.004
Bond angles (°)	1.193	1.019	1.135	0.650
Validation				
MolProbity score	2.02	1.79	1.98	1.20
Clashscore	3.73	4.08	4.03	4.15
Poor rotamers (%)	5.84	3.42	4.63	1.02
Ramachandran plot				
Favored (%)	95.97	96.89	95.84	96.66
Allowed (%)	3.78	3.02	3.78	3.34
Disallowed (%)	0.25	0.08	0.34	0

*Determined with cryoSPARC.